www.ietdl.org

Published in IET Renewable Power Generation
Received on 11th July 2011
Revised on 23rd March 2012
doi: 10.1049/iet-rpg.2011.0188

ISSN 1752-1416

Solar dish-Stirling system optimisation with a doubly fed induction generator

D. Santos-Martin J. Alonso-Martinez J. Eloy-Garcia S. Arnalte

Department of Electrical Engineering, University Carlos III, Madrid, Spain
E-mail: dsmartin@ing.uc3m.es

Abstract: A handful of dish-Stirling system designs, comprising different solar concentrators and Stirling engine/generators, are currently and successfully demonstrating the technical feasibility of solar power generation for extended periods of time. Most designs focus on concentrators and engines obtaining a high performance while remaining robust. The systems achieve power control by varying gas pressure or engine volume. This study shows how to optimise the power generation of grid connected dish-Stirling systems by varying the Stirling engine speed when coupling it to a doubly fed induction generator (DFIG). The proposed control system for DFIG is direct power control, which performs the tracking of the maximum power point within the Stirling engine characteristic.

1 Introduction

Over the last two decades, large-scale integration of renewable energy has become a fact because of social and geopolitical concerns. Solar thermal energy, also known as concentrating solar power (CSP), is emerging as an important response to new demands for clean, renewable electricity generation. Three solar thermal systems, commonly referred to as power tower, trough and dish-Stirling (DS), are used to produce electricity.

The most mature CSP technology is the trough-electric system, with hundreds of MW up and running. This system produces about 75 suns concentration and operates at temperatures of about 400°C at an annual efficiency of about 10%, depending on solar potential. Solar power towers are also in use as a feasible alternative as they operate at a concentration of 800 suns, and produce temperatures of about 560°C with an efficiency of about 15%. The least deployed, on the other hand, is the DS system, although it produces 3000 suns concentration and operates with temperatures around 750°C and annual efficiencies of 23% [1–3].

Research into DS technology has been ongoing for more than 20 years [2–5], although the system is still considered relatively new. The first large plant to use DS technology began operating in Arizona in January 2010 with an overall installed capacity of 1.5 MW. Various other plants rated for several hundred MW are currently in the planning stages in California [6].

DS systems track the sun and focus solar energy onto a thermal receiver integrated in the Stirling engine. The receiver consists of a heat exchanger designed to transfer the absorbed solar energy to the working fluid, typically hydrogen (helium or air are an alternative). The Stirling engine then converts the absorbed thermal energy into mechanical power by expanding the gas in a piston-cylinder. The linear motion is usually converted to rotary motion in order to turn a generator that produces electricity. The main DS components are: concentrator, receiver, power conversion unit, orientation drive and mechanical structure.

One disadvantage of DS systems is that they can use only the direct component of the solar radiation because the diffuse component cannot be concentrated on the receiver because of their high-concentration ratios [7], typically more than 1000 suns.

Most DS systems to date have incorporated kinematic Stirling engines, where both the power piston and the displacer are mechanically (kinematically) linked to a rotating power output shaft where a generator is mounted [1].

Another option is the free-piston engine [3], which only has two moving parts, the displacer and the power piston, that bounce back and forth between springs. A linear alternator is attached to the piston to extract work from the cycle. Stirling engines are preferred for this application mainly because of their high thermal-to-mechanical efficiency, in excess of 40% [3].

Real Stirling engines show very weak output compared to their excellent theoretical yield. In fact, these engines have complex phenomena related to compressible fluid mechanics, thermodynamics and heat transfer. Many studies are currently taking place to accurately describe and understand these highly non-stationary phenomena, with the aim to determine the different engine losses, optimal performance and design parameters involved. Some of these works can accurately predict actual Stirling engine performance, particularly with regard to efficiency and output power [8]. These analyses clearly show the dependence of power losses and output power as functions of the operating frequency [9].

Taking into account the importance of the Stirling engine operating frequency within the power losses [8–10], this

paper shows how to optimise the power generation in grid connected DS systems by means of varying the Stirling engine speed when coupling it to a doubly fed induction generator (DFIG). The proposed control system for the DFIG is direct power control (DPC) which performs the tracking of the maximum power point of the Stirling engine characteristic.

2 Review of outstanding DS systems and projects

From the mid-1980s to the mid-1990s a number of different solar DS systems ranging in size from 5 to 50 kW were built in the USA, Germany, Spain and Japan [5, 11], mainly for demonstration purposes.

According to Poullikkas *et al.* [11] there are currently nine operational solar dish systems around the world, with plant ratings from 3 kW by Infinia Corp. and 10 kW by Schlaigh–Bergermann and Partner up to 150 kW by Stirling Energy Systems or Wizard Power Pty.

There are four large projects currently under planning and construction that are worth highlighting because of their significant power size. Three of these projects use Stirling Energy Systems technology and are located in the USA (California and Arizona) with an installed capacity of 1.5, 750 and 850 MW. The fourth is to be installed in India using Infinia Corp. Technology and will have a capacity of 9–10 MW.

The older projects have used [1] the following DS systems: (i) SAIC/STM SunDish System, (ii) Schlaich–Bergermann und Partner Eurodish and (iii) WG Associates'Advanced Dish Development System. The current DS systems under commercial development are: (i) Stirling Energy Systems' DS System (ESE-Tessera) and (ii) PowerDish by Infinia Corp.

A summary of the main characteristics of these DS systems is shown in Table 1 [1], with five systems that are connected to the grid and one that works in standalone operation. The different types of Stirling engines used are: STM 4-120, Solo 161, Kockums/SES and Infinia (free-piston). Products under current commercial development are: SES which drives a 'fixed speed' conventional three-phase induction generator of 480 V, and Infinia which has a different approach driving iron linear generator.

As shown by the Beale or West equations [3] the maximum power output of a well-developed Stirling engine is roughly proportional to pressure, volume and speed. Table 1 [1] shows how one system achieves power control by varying the angle of the swashplate and therefore the volume, whereas most of the others vary the working gas pressure. None use the capability of controlling the power of grid connected systems by means of varying the speed of the engine. The operating speed for the grid connected systems is summarised in Table 2.

3 Power-speed Stirling engine characteristic

Considering the Stirling engine, the dynamics of the heater temperature can be obtained from the energy balance of the system, where the input thermal energy results in a temperature variation plus the thermal losses and thermal energy absorbed by the Stirling engine heater. An increase in the direct component of the insolation causes a temperature increase and therefore requires an increase in the absorbed Stirling engine energy in order to counteract. This increase in absorbed energy is typically achieved by increasing the pressure inside the engine, which in turn increases the total working gas quantity and allows the engine to absorb more heat. A decrease in insolation, on the other hand, requires a decrease in pressure to maintain the heater temperature.

The power of Stirling engines can be controlled by varying the temperature, pressure, stroke, phase angle dead volume and speed. The typical strategy when insolation is high enough, as used by DS systems described in the previous overview, is to control the pressure or stroke so that the temperature remains constant at the maximum design level and the Stirling engine functions at optimal efficiency levels.

As presented in many experimental research projects [12–19] with Stirling engines, measurements show that when using constant values of internal parameters (such as temperatures and/or engine displacement) the engine

Table 1 comparative specifications and performance parameters for ds systems [1]

Power Conv. Unit	SAIC/STM	SBP	WGA ADDS*	WGA standalone	SES	Infinia Corp.
aperture dia, cm	38	15	14	14	20	4.5
engine type	STM 4-120 kinematic	SOLO 161 kinematic	SOLO 161 kinematic	SOLO 161 kinematic	Kockums/SES 4-95 kinematic	PowerDish Free-piston
no. cylinders, cc	4	2	2	2	4	1
	480	160	160	160	380	–
operational speed, rpm	2200/1800	1500	1800	800–1890	1800	–
working fluid	hydrogen	helium	hydrogen	hydrogen	hydrogen	helium
power control	variable stroke	variable pressure	variable pressure	variable pressure	variable pressure	–
generator	3φ/480/Induct	3φ/480/Induct	3φ/480/Induct	3φ/480/Sync.	3φ/480/Induct	Linear
system information	SAIC/STM	SBP	WGA ADDS	WGA standalone	SES	
no. systems built	5	11	1	1	70	1
on-Sun Op., h	6360	40 000	4000	400	–	–
rated output, kW	22.9	8.5	11	8	25.3	3.2
peak efficiency, %	20	19	24.5	22.5	29.4	24
Ann. efficiency net, %	14.5	15.7	18.9	–	24.6	–
Ann. energy, kW h	36 609	20 252	17 353	–	48 129	–

[a]WGA ADDS: Sandia Laboratory system built by WGA

Table 2 DS speed data for grid connected systems

DS system	Stirling engine	Operation speed (grid frequency)	Generator type (no. of pair of poles)
SAIC/STM	STM 4-120	2200/(gearbox)/1800 (60 Hz)	induction generator (2pp)
SBP	SOLO 161	1500 (50 Hz)	induction generator (2pp)
SES	Kockums/SES 4-95	1800 (60 Hz)	induction generator (2pp)
WGA (Mod1)	SOLO 161	1800 (60 Hz)	induction generator (2pp)

develops a cycle-averaged torque value that varies with the engine speed (see Table 3). All these studies conclude that an increase in speed results in a decrease in heat exchange time and an increase in flow losses, and therefore obtains a negative slope in torque. When reasoning in terms of power, a decrease in shaft power is produced after the maximum point as a result from the same effects of friction and inadequate heat transfer at higher speed. It is known that the output torque is significantly affected by the pressure loss of the working gas and mechanical loss because of friction. Moreover, pressure loss is affected by the engine type and operating conditions such as engine speed. It has also been confirmed in analytical models [10] that at constant operating conditions the output torque decreases at an increasing speed, caused by a rise in pressure loss in the heat exchangers and mechanical loss caused by viscosity friction. Thus, there is an optimal engine speed at which maximum output power is obtained.

Although the cited experimental research references are for high/low temperature and low pressure, the same physical effects described above to justify the decreasing torque-speed characteristic are expected in DS-systems working under high-temperature and high-pressure conditions (1000 K, 200 bar). Senft [9] explains how the engine operating frequency affects not only the indicated power but also the mechanical efficiency and becomes an important factor for optimisation purposes.

Moreover if the insolation varies, a set of torque-speed characteristics is obtained. The torque-speed characteristics referred in Table 3 can be approximated by a linear model, as shown in Fig. 1. This assumption is valid for a wide range of speeds.

Therefore assuming a decreasing linear model for the torque-speed characteristic, as shown by all the references in Table 3, with fixed insolation conditions yields

$$T(\Omega) = -m_i \cdot \Omega + T_0 \tag{1}$$

where T is the engine torque, Ω is the shaft speed, T_0 is the extrapolated torque at zero speed and m_i is the slope; both T_0 and m_i vary with the internal energy or heat.

In order to model the energy exchange it is necessary to express the thermodynamic and heat transfer differential equations of the Stirling engine within the main parts: heater, regenerator, cooler and working spaces. A very simplified approach would consider the net instantaneous heat rate transfer to the Stirling cycle as a first-order system with a mean time response that represents the overall thermal inertia as shown in

$$Q(t) = Q_0 \cdot (1 - e^{-(t/\tau)}) \tag{2}$$

where Q is the net absorbed heat rate by the Stirling cycle, Q_0 represents the steady-state value (dependant, among others, on the insolation) and τ is the time response of the system.

When considering parameters m_i and T_0 proportional to the engine heat rate if the insolation varies, a set of torque-speed characteristics is obtained (Fig. 1), where the transition from one curve to the other depends on the thermal inertia.

The set of power-speed characteristic curves (3) can be derived by simply multiplying the torque and the speed, which results in a quadratic curve with a maximum power point (Fig. 2)

$$P(Q, \Omega) = T \cdot \Omega = -m_i(Q) \cdot \Omega^2 + T_0(Q) \cdot \Omega \tag{3}$$

Since the brake thermal efficiency is the shaft power divided by a constant heat rate input, for each insolation the curve of brake thermal efficiency has the same trend as the shaft power and for each curve the peak efficiency point is obtained at an optimal speed (Ω_{opt}) value that can be obtained from (4)

$$\frac{\partial P}{\partial \Omega} = -2m_i \cdot \Omega + T_0 = 0 \tag{4}$$

$$\Omega_{opt} = \frac{T_0}{2m_i} \tag{5}$$

The corresponding power (P_{max}) for the optimal speed for a given insolation is

$$P_{max} = \frac{T_0}{2}\Omega_{opt} \tag{6}$$

Fig. 2 also shows the locus of peak power points for each insolation value.

It is important to note that DS systems typically have a pressure system that works at maximum heater temperature without exceeding the maximum operating limits for

Table 3 Experimental data for stirling engine power-speed characteristic while varying the heating temperature

Stirling engine (type)	Temperature range, K	Optimal speed range, rpm	Gas (pressure)	Reference
α	1023–1373	290–500	air (2.5 bar)	in [16] see Fig. 8
ß	800–1000	152–220	air (1 bar)	in [13] see Figs. 4 and 6
γ	399–436	40–50	air (1 bar)	in [14] see Figs. 11 and 12
γ	401–439	19–21	air (1 bar)	in [15] see Figs. 9 and 10
γ	507–589	100–130	air/helium (3.4 bar)	In refences [12/18] see Figs. 8/9
γ	900–1000	700–900	air (2.5 bar)	in [17] see Figs. 6 and 7

doi: 10.1049/iet-rpg.2011.0188

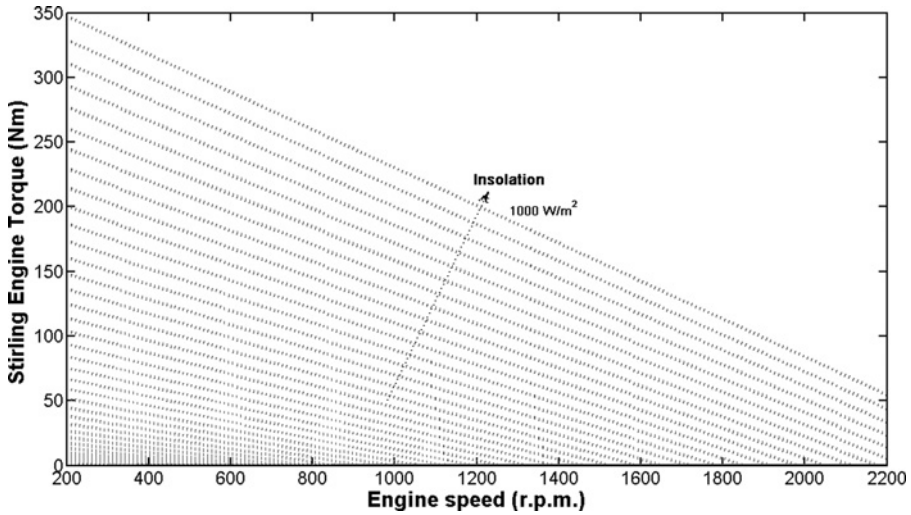

Fig. 1 *Stirling engine linear torque-speed characteristic for different insolation values (30 W/m^2 step)*

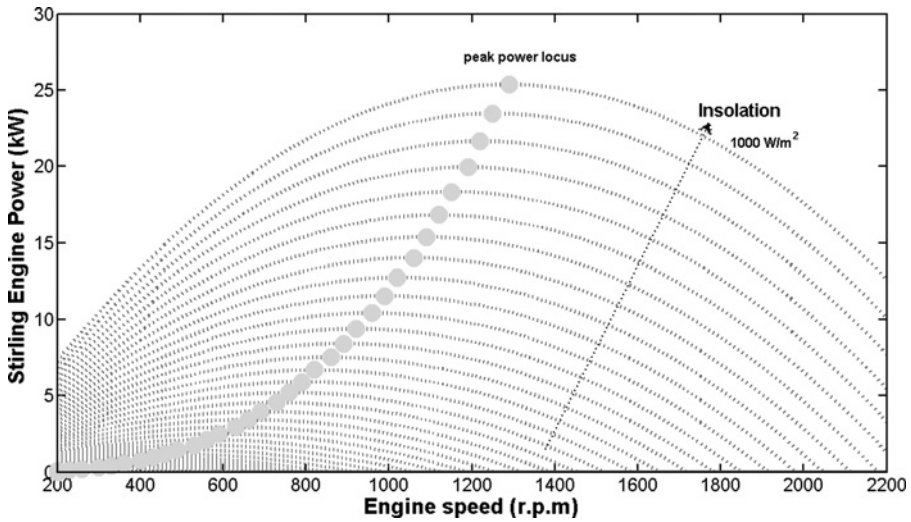

Fig. 2 *Stirling engine steady-state model (power–speed) for different insolation values (30 W/m^2 step)*

pressure and temperature. Considering the speed as a new control variable would add a new degree of freedom to allow the optimisation process at any operating condition.

4 DPC applied to DFIG

In electrical terms, the evolution of short-circuit induction generators and wound rotor induction generators with supersynchronous cascade has reached its maturity with the introduction of DFIG with bidirectional, and partially rated, power flow inverters. The application of well-known control techniques, such as flux oriented vector control, has proved to be sufficient for the accomplishment of the initial requirements, although it also involves significant drawbacks because of its linear nature, such as lack of robustness when facing parameter changes and/or changes in operating conditions.

The application of modern control techniques based on state variable analysis, that is, pole placement, linear quadratic regulators and robust control designs such as linear-Gaussian or singular-value-based solutions like H_∞, on motor or generator control has not proved popular. Non-linear control techniques, such as direct torque control (DTC), have been proposed over the last decades [20] because of both the non-linear nature of the inverter, with a finite number of states, and the linear time-varying nature of the machine model. The basic principle of DTC is the selection of a space vector and an average control signal to instantaneously control, during one sampling period, both the electromagnetic torque and the flux magnitude.

DPC applied to DFIG is based on the same concept as DTC, but it controls stator active and reactive power directly, instead of torque and rotor flux [21].

In DFIGs the rotor side inverter, working as a voltage source, controls the stator active and reactive power directly, by means of the rotor flux and by applying the appropriate voltage vector.

Both active and reactive powers are scalar magnitudes, with definitions that are independent of the reference system

$$\begin{aligned} P_s &= \overline{u}_s \cdot \overline{i}_s \\ Q_s &= |\overline{u}_s \times \overline{i}_s| \end{aligned} \tag{7}$$

The DFIG stator and rotor flux linkage vectors can be defined

for any static or rotating reference as

$$\begin{aligned}\overline{\boldsymbol{\phi}_S} &= L_S\overline{\boldsymbol{i}_S} + L_m\overline{\boldsymbol{i}_R}\\ \overline{\boldsymbol{\phi}_R} &= L_R\overline{\boldsymbol{i}_R} + L_m\overline{\boldsymbol{i}_S}\end{aligned} \tag{8}$$

where L_s, L_r, L_m are the stator, rotor and mutual inductance, respectively.

The stator current can be expressed as

$$\begin{aligned}\overline{\boldsymbol{i}_S} &= \frac{1}{\sigma L_s}\left(\overline{\boldsymbol{\phi}_S} - \frac{L_m}{L_r}\overline{\boldsymbol{\phi}_R}\right)\\ \sigma &= 1 - L_m^2/(L_sL_r)\end{aligned} \tag{9}$$

where σ is the leakage factor.

By taking into consideration or neglecting the stator resistance, an exact or an approximate expression can be obtained as follows

$$\begin{aligned}P_s &= \frac{1}{\sigma L_s}\overline{\boldsymbol{u}_s}\left(\overline{\boldsymbol{\phi}_S} - \frac{L_m}{L_r}\overline{\boldsymbol{\phi}_R}\right) \simeq \frac{L_m}{\sigma L_rL_s}|\overline{\boldsymbol{u}}_s||\overline{\boldsymbol{\phi}}_R|\cos(\theta_R)\\ Q_s &= \left|\frac{1}{\sigma L_s}\overline{\boldsymbol{u}_s} \times \left(\overline{\boldsymbol{\phi}_S} - \frac{L_m}{L_r}\overline{\boldsymbol{\phi}_R}\right)\right|\\ &= \left|\frac{1}{\sigma L_S}\left(|\overline{\boldsymbol{u}}_s||\overline{\boldsymbol{\phi}}_S|\sin(\theta_S) - \frac{L_m}{L_R}|\overline{\boldsymbol{u}}_s||\overline{\boldsymbol{\phi}}_R|\sin(\theta_R)\right)\right|\end{aligned} \tag{10}$$

As shown in (10), considering $|\overline{u}_s|$ and $|\overline{\phi}_S|$ as constant values, the variation of the angle between the rotor flux and the stator voltage, and the variation of the rotor flux modulus will produce increments in the stator active and reactive powers (Fig. 3).

Giving the usual angle $\theta_R \simeq \pi/2$ and any small variations of the angle will mainly affect the active power and, by contrast, variations on the modulus of the rotor flux will primarily affect the reactive power. Considering (11), the rotor voltage may modify, within each sampling period, the angle and modulus of the rotor flux and, therefore also the active and reactive powers in the desired way. For a two level converter, six active vectors (V_1, …, V_6) and two non-active vectors (V_0, V_7) are possible

$$\Delta\overline{\boldsymbol{\phi}}_R^R = (\overline{\boldsymbol{u}}_R^R - R_R\overline{\boldsymbol{i}}_R^R)\tau \simeq \overline{\boldsymbol{u}}_R^R\tau \tag{11}$$

where τ is the switching period.

The DPC strategy is based on these assumptions and summarises on a table the effects of the rotor voltage on the evolution of the stator active and reactive powers, predicting for every 60° sector the most convenient vector to be applied in order to increase or decrease the power. Two hysteresis controllers, that compute signals in power error, feed the necessary input to the table. As shown in Fig. 3, the DPC strategy is defined to apply the same vector during a 60° sector. This classical strategy can be improved by using a 30° sector, as the vectors that maximise the changes in the active and reactive powers are the same only for a 30° sector, because of the 30° displacement between power increment patterns.

The proposed control DPC system is made of different modules which calculate: (i) the stator voltage components and its angle in real time, (ii) the active and reactive power and (iii) the power error, in order to feed the hysteresis regulators and obtain the optimal active rotor vector (V_{1-6}) to be applied by the optimal switching table (Table 4).

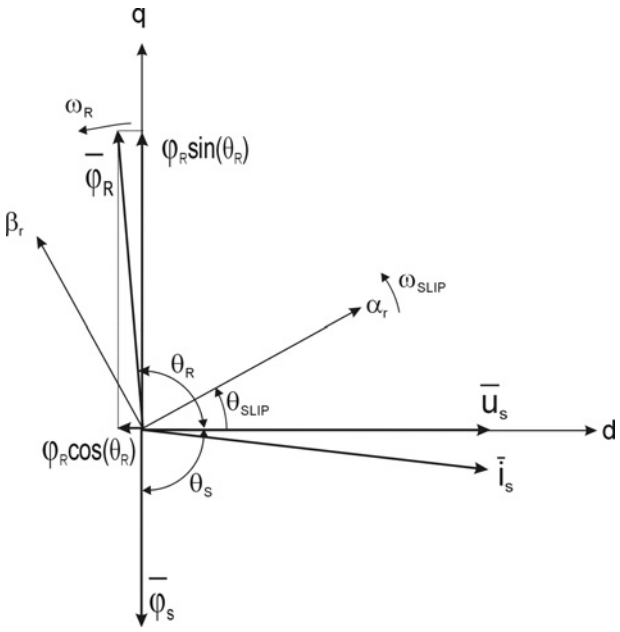

Fig. 3 *Stator voltage and rotor flux linkage vectors and its projections with synchronous reference dq*

5 Maximum power point tracking with a DFIG

The use of a DFIG allows to decouple the generator speed (ω) from the constant grid pulsation (ω_S), by means of injecting a rotor current with a pulsation (ω_R) which is the difference between the two previous pulsations (12), making this generator a good option when a variable speed system is desired

$$\begin{aligned}\Omega &= 60\omega/P_p\\ \omega_S &= \omega_R + \omega\\ s &= (\omega_S - \omega)/\omega_S\end{aligned} \tag{12}$$

where Ω is the mechanical rotating speed, P_p is the generator pair of poles and s is the slip ratio.

As shown in Fig. 4, the total active power injected into the grid (P_g) is the sum of the power delivered through the stator (P_S) and through the rotor (P_R) [22]; furthermore, it can be demonstrated that the share is a function of the rotor speed or the slip ratio.

The modelling of the rotational system (Stirling engine and DFIG) may be simplified into a single equation of motion

$$T_{st-}T_G = J\,d\Omega/dt + D_f\Omega \tag{13}$$

Table 4 Optimal switching table for DPC

		Sector 1	Sector 2	Sector 3	Sector 4	Sector 5	Sector 6
Ps ↑	Q_s ↓	2	3	4	5	6	2
	Q_s ↑	3	4	5	6	1	2
Ps ↓	Q_s ↓	6	1	2	3	4	5
	Q_s ↑	5	6	1	2	3	4

doi: 10.1049/iet-rpg.2011.0188

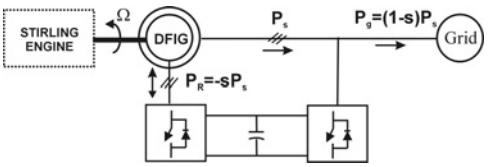

Fig. 4 *Power flow of a DFIG coupled to a Stirling engine*

where Ω is the Stirling engine-generator speed (rad/s); T_{st} is the effective mechanical torque provided by the Stirling engine (N m); T_G is the electromagnetic torque applied on the generator shaft (N m); J is the sum of the Stirling engine and DFIG rotor inertia (kg m^2); and D_f is the sum of the Stirling engine and DFIG friction coefficients (N m/rad).

Therefore the speed of the Stirling engine-generator can be controlled by adjusting the electromagnetic torque on the generator shaft. The required torque variation can be implemented using the DPC technique as previously explained.

Two strategies are presented to reach the optimal speed and therefore the maximum power point tracking (MPPT).

5.1 Open-loop MPPT

Here, for a particular irradiance, a speed reference that achieves maximum power is calculated by means of the power-speed Stirling engine characteristic and passed on to a speed controller. The speed controller will set a power reference for the electrical generator. Balance between Stirling engine torque and generator torque will result in an accelerating torque until the desired speed is achieved.

When regulating the system under the specification of maximum power, it must be taken into account that DS power must never be higher than the rated electrical power. At this point (rated irradiance), the control strategy has to change so that a higher irradiance no longer produces optimum power but rated power. This can be achieved by changing the speed in order to reduce the performance and by maintaining the power at its rated value. Fig. 5 shows the control system diagram.

5.2 Perturbation and observe (P&O) MPPT

The P&O algorithm operates by periodically perturbing (i.e. incrementing or decrementing) the system speed and comparing the DFIG output power with that of the previous perturbation cycle. If the DS operating speed changes and the power increases, the control system moves the DS operating point in that direction; otherwise the operating point is moved in the opposite direction. In the next perturbation cycle the algorithm continues in the same way.

Two approaches can be taken: either the perturbation of the DS operating point has a fixed magnitude, or an average of several samples of the DS power is used to dynamically adjust the perturbation magnitude of the DS operating point. This work considers a fixed perturbation magnitude (Fig. 6).

6 Modelling and simulation results

A complete model of the DS system has been implemented including: one mass mechanical model, a Stirling engine model and a DFIG model with a DPC controller and both MPPT controllers (Figs. 5 and 6). All parameter values are summarised in the Appendix.

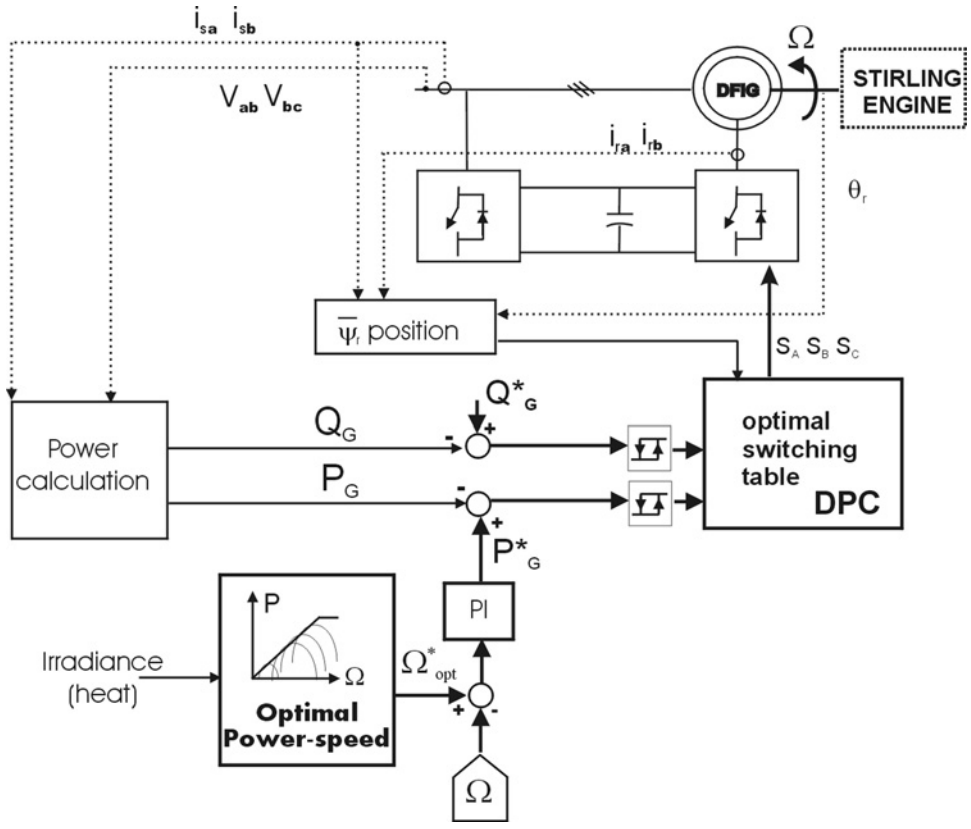

Fig. 5 *Schematic diagram of the open-loop MPPT and DPC algorithm*

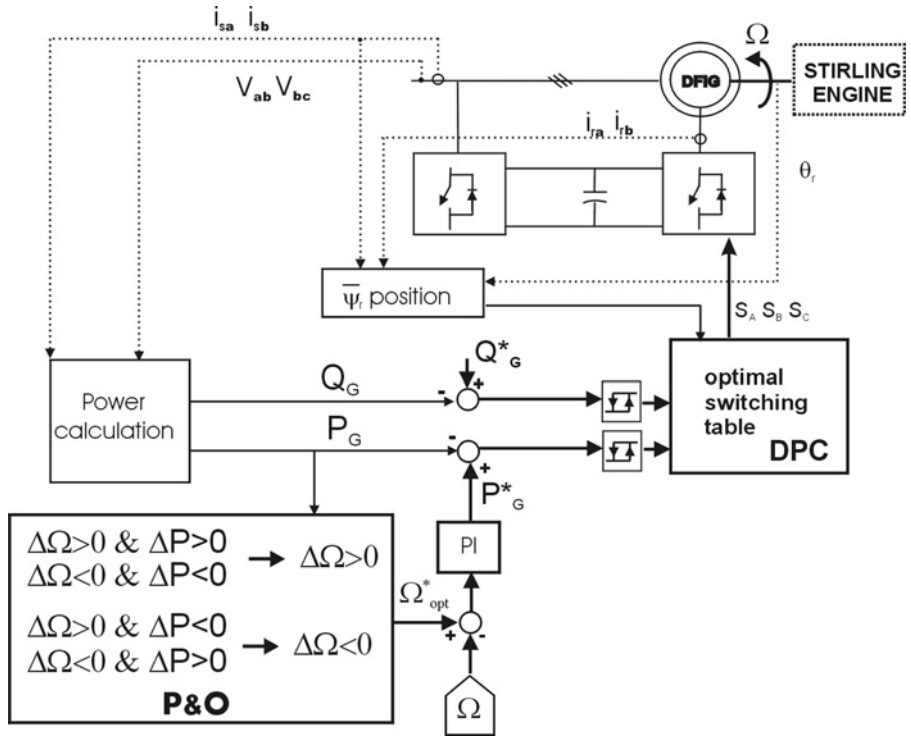

Fig. 6 *Schematic diagram of the P&O MPPT and DPC algorithm*

6.1 Mechanical model

The well-known one-mass model in per unit values is modelled as

$$T_{st\_}T_G = 2H\,\mathrm{d}\Omega/\mathrm{d}t + D\Omega \tag{14}$$

where H and D are the inertia and friction coefficients in per unit values, respectively.

When multiplying (14) by Ω, it yields a linear equation if a variable change is applied with $x = \Omega^2$

$$P_{st\_}P_G = H\,\mathrm{d}x/\mathrm{d}t + Dx \tag{15}$$

where P_{st} and P_G are the Stirling and DFIG power, respectively, and x the square of the mechanical speed. This model is shown as a block diagram and Laplace variable in Fig. 7.

6.2 Stirling engine model

The Stirling engine has been modelled by its power-speed characteristic presented as a set of curves where the mean power within a cycle (3) is a function of the net absorbed heat rate (insolation) with dynamics that have been simplified by using a first-order model (2) to consider the overall thermal inertia. It has been implemented as a look-up table performing linear 2D interpolation (Fig. 2) and a first-order model that varies parameters m_i and T_0 which 'jump' dynamically among curves when an insolation change occurs.

Fig. 7 *One-mass mechanical model in Laplace variable*

6.3 DFIG model with DPC

The DFIG with DPC is implemented considering a full model [20, 21]. As shown in Fig. 8, this non-linear controller has extremely high dynamics, with time responses of about 1 ms, and is therefore highly convenient when perturbations occur. Active and reactive power control can be controlled independently. Fig. 8 shows an example. First a change in the active power is produced while maintaining constant reactive power. Then a change in the reactive power is produced while maintaining constant active power.

6.4 MPPT controllers

Both MPPT controllers (open-loop and P&O) have a speed control loop. A PI controller assures that there is not steady-state error in the speed (Figs. 5 and 6). To tune the controller parameters the plant pole has been cancelled and a time response of 1 s has been specified, with no overpass, while the DFIG/DPC system is modelled by a unity gain because of its extremely fast response without error (see PI parameters in the Appendix). A feedforward term has been added to the control law to cancel the insolation disturbance over the speed control loop (Fig. 9).

The open-loop MPPT measures the irradiance value and knowing the optimal characteristics, sets the reference for optimal speed.

In contrast to the open-loop MPPT, the P&O MPPT does not need to measure the irradiance. A small perturbation is added to the speed reference, $\Delta\Omega(k)$, and then observing the power response, $\Delta P(k)$, the maximum power point is tracked, according to Table 5, with a small ripple. To achieve this, the measured power is averaged within a running window, T. This time value and the constant speed perturbation (Δ_{speed}) are shown in the Appendix.

doi: 10.1049/iet-rpg.2011.0188

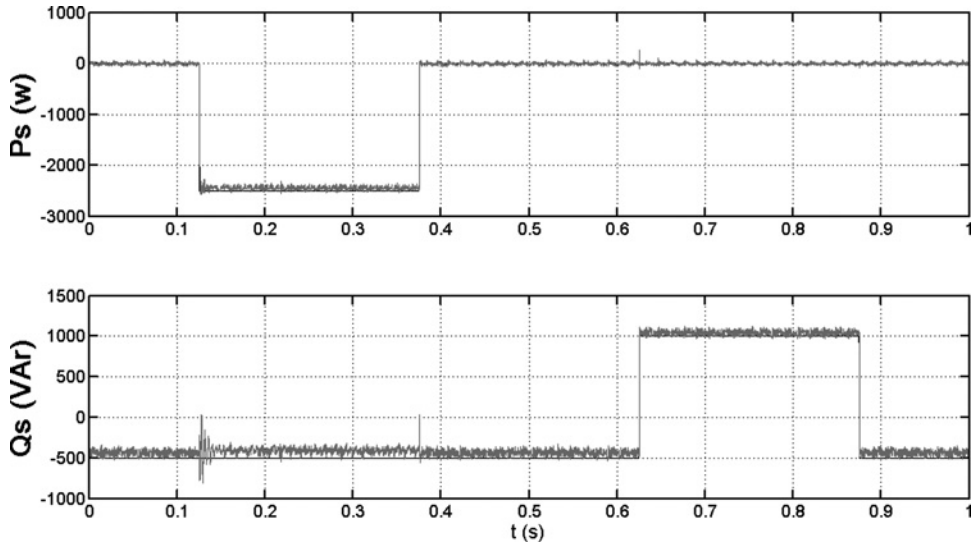

Fig. 8 *DFIG with DPC response to active power (P_S) and reactive power (Q_S) commands*

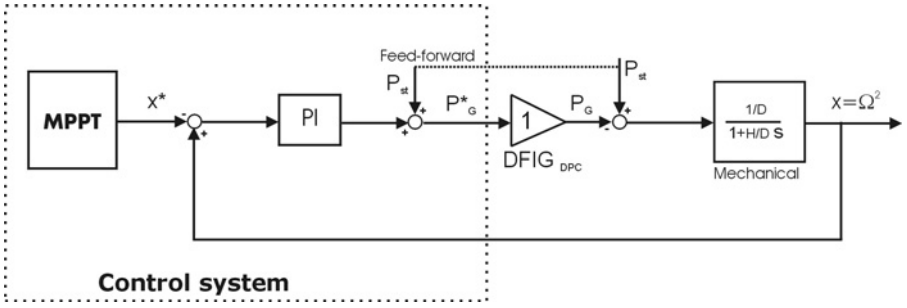

Fig. 9 *Schematic control loop*

Table 5 Logic table for the P&O mppt (0 = false, 1 = true)

$\Delta\Omega(k+\tau)$	$\Delta P(k) \leq 0$	0	1
$\Delta\Omega(k) \leq 0$	–	–	–
0	–	Δ_{speed}	$-\Delta_{speed}$
1	–	$-\Delta_{speed}$	Δ_{speed}

Outcome corresponds to the speed perturbation to be applied $\Delta\Omega(k+\tau)$

6.5 Case study

A number of simulation results were obtained in order to show the convenience of operating the grid connected DS at variable speed instead of at fixed speed, as it is usually done. Moreover, these results validate the performance of the proposed power controllers of the DS system with DFIG.

Figs. 10 and 11 show system response to a step in insolation for both of the presented MPPT strategies, P&O (Fig. 10) and open loop (Fig. 11).

At $t = 0$, the system is in steady-state operation, with an insolation of 1 kW/m^2. At this point, the relative efficiency (output electric power/input heat rate) shown in the figures is very close to 100%, which means that the system is operating at the maximum power point.

At $t = 20$ s, a step in insolation is simulated, reducing the simulated insolation from 1 to 0.5 kW/m^2. As it can be seen, the heat rate does not change abruptly, because of the thermal inertia of the system. Instead, a smooth transition is observed (Figs. 10*a* and 11*a*).

During this transient, the MPPT algorithm detects that the system is no longer at the maximum power point and modifies the speed reference for the DFIG speed controller in order to extract the maximum available power (Figs. 10*b–d*) and 11*b–d*). As it can be seen, the relative efficiency of the MPPT algorithm is very close to 100% even during the transient period (Figs. 10*e* and 11*e*). After a few seconds, the system reaches stable operation at the maximum power point that corresponds to the new insolation value.

At $t = 60$ s, a new step in insolation is introduced in the opposite direction, from 0.5 to 1 kW/m^2. As it can be seen, the system effectively tracks the maximum power point, quickly reaching a relative efficiency of 100% (Figs. 10*e* and 11*e*).

Comparing the results of the two presented MPPT algorithms, it can be seen that both are able to track the maximum power point with a similar effectiveness. A somewhat higher ripple in relative efficiency can be observed for P&O method, which can be considered as a drawback. However, it has to be noted that the open-loop method is heavily dependent on model accuracy, and therefore some errors, even steady-state errors, are to be expected in a real setup. The perturb and observe approach does not rely on model accuracy and therefore such errors are not expected to occur.

Fig. 12 shows the same results as Fig. 10 but representing only electrical power against engine speed, therefore discarding all time information. In that figure, the characteristic curves of the system are also represented for various levels of heat rate, therefore representing the possible operating points of the system.

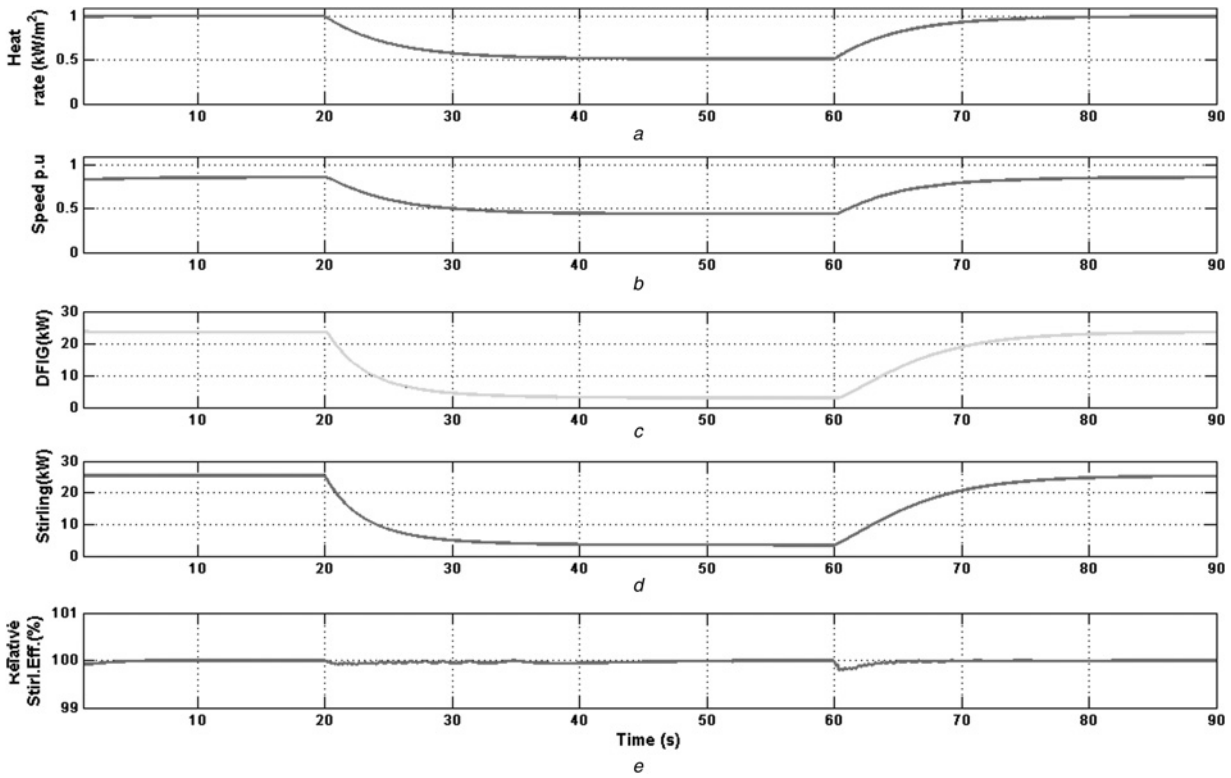

Fig. 10 *Dynamic response with MPPT (open-loop) during a heat rate (insolation) change (from top to bottom)*

a Heat rate
b Speed
c DFIG output power and reference
d Stirling power
e Relative electric efficiency

At $t = 0$ the system is operating at point 1, which is the maximum power point for the given heat rate. During the first transient between $t = 20$ and 60 s, the state of the system gradually changes from point 1 to point 2 along the path that is highlighted in the figure. As the response in power is likely slower than the response in speed, the controller manages to nearly track all the maximum power points between the maximum insolation value (point 1) and a lower one (point 2).

During the second transient, from $t = 60$ s onwards, the system returns from point 2 to point 3, which is the same as point 1, since the insolation conditions are the same.

It is important to note the difference between working at variable speed (points 1–2–3) and working at fixed speed (points 1–2b–1). It is clear that both options would yield different power performance, in the given example the system hardly produces any power at reduced insolation at constant speed operation. Moreover, it is true that fixed speed operation can be further optimised from what is shown in Fig. 12, but since at variable speed the maximum power point is constantly tracked; fixed speed performance would be inevitably lower. In case of choosing the variable speed option this choice corresponds to a wide range of speeds, typically for this type of generator with a ratio of 3:1 (high speed:low speed).

Figs. 13 and 14 show the simulation results using the modelled DS system with the proposed controllers using as input a 1-day real insolation data in two different situations: sunny day and a cloudy day with high insolation. The objective of this analysis is to validate the controllers when facing real insolation changes. It is important to note that DS system only uses the direct component of the solar radiation. The speed of radiation rate changes is typically rather slow (<0.5% per minute for the data in Fig. 13) during the sunrise and sunset. Nevertheless in cloudy conditions, this speed can be much higher. For example, in the insolation data of Fig. 14 it reaches 25% per minute. It can be stated that when designing controllers for such a system, in clear atmospheric conditions, the dynamics of the plant will be excited slowly by the insolation change but during a cloudy day these changes can be unpredictable. Therefore testing the control algorithm response to a step change, as done in Figs. 10–12, is the only way to ensure that the maximum power is going can be extracted under any atmospheric change.

The insolation data details used in Figs. 13 and 14 are summarised in the Appendix.

Fig. 13 shows system response to a sunny day with real insolation data using the presented open-loop MPPT strategy. At $t = 7$ h, sun starts rising and the insolation increases with the typical slope for a sunny day until a maximum value with a total measured insolation of 990 W/m^2 and an estimated direct irradiance of 722 W/m^2 which is concentrated by the DS sytem to produce power. During the initial time the Stirling engine starts accelerating but because of the modelled torque-speed characteristic the effective output power for the engine and thus for the generator is still negligible. After 8:30 hours the MPPT algorithm detects that the system is capable of producing effective power and modifies the speed reference for the DFIG speed controller in order to extract the maximum available power (Fig. 13*b*). As it can be seen, the relative efficiency of the MPPT algorithm is very close to 100% and nearly during the whole day even during the

doi: 10.1049/iet-rpg.2011.0188

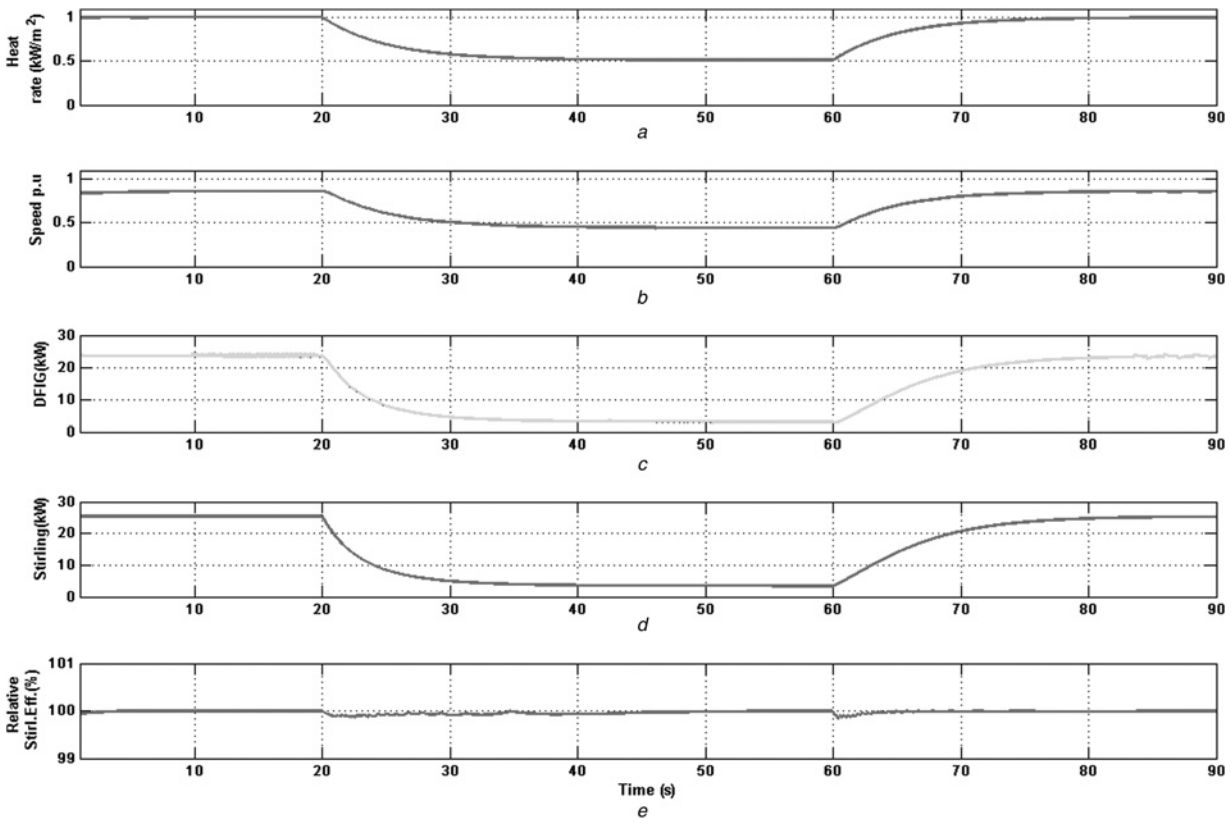

Fig. 11 *Dynamic response with MPPT (P&O) during a heat rate (insolation) change (from top to bottom)*

a Heat rate
b Speed
c DFIG output power and reference
d Stirling power
e Relative electric efficiency

transient period (Figs. 13*e*). During the sunset the inverse process is observed for the speed and output power, with just a small ripple in the efficiency at very low power values.

Fig. 14 shows system response to a cloudy day with real insolation data using again the presented open-loop MPPT strategy. At $t = 7$ hours, sun starts rising and the insolation increases but the atmospheric conditions produce irregular insolation changes. As for the sunny day when the effective generated power compensates losses, after 10 h (Figs. 14*c* and *d*), the MPPT algorithm modifies the speed reference for the DFIG speed controller in order to extract the maximum available power and the relative efficiency reaches 100% (Fig. 14*e*). During the rest of the day it can be observed how the DS system with the proposed controller shows an optimal performance following any type of insolation changes, reaching for that day a maximum speed radiation rate of 25%

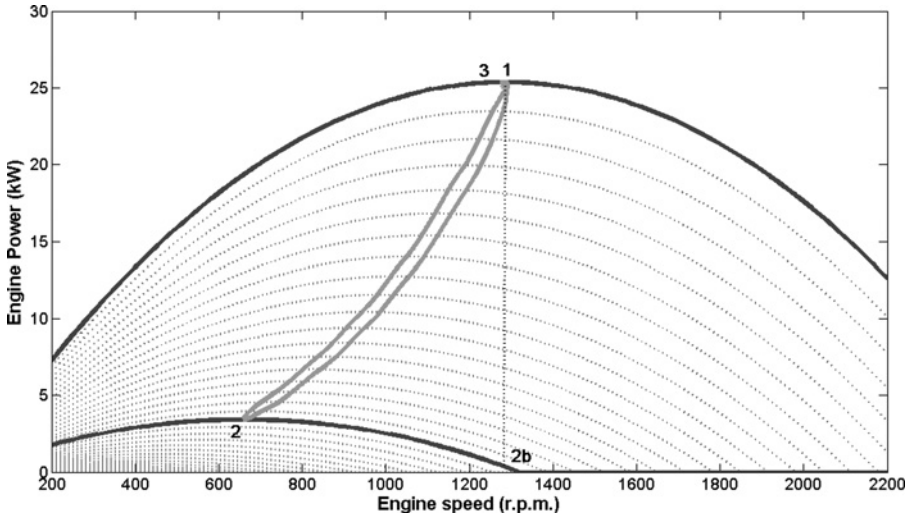

Fig. 12 *Stirling engine power evolution for different insolation values with MPPT in open loop*

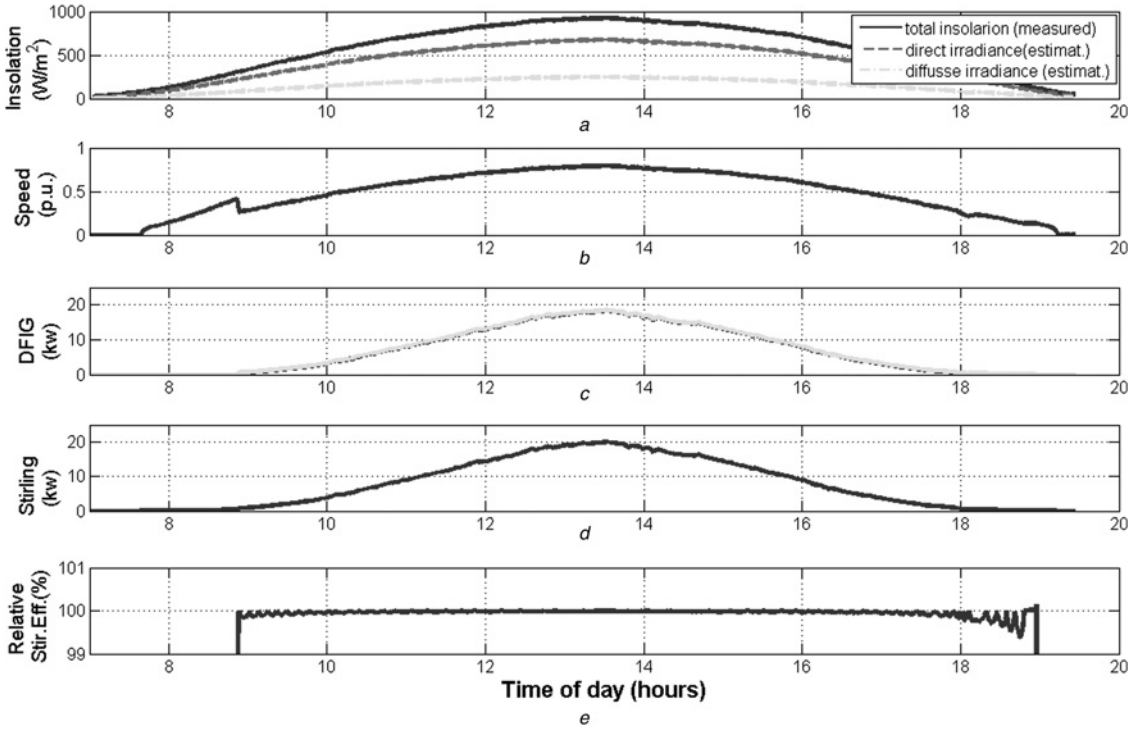

Fig. 13 *Dynamic response with MPPT (open loop) for real insolation data of one sunny day (from top to bottom)*

a Insolation
b Speed
c DFIG output power and reference
d Stirling power
e Relative electric efficiency

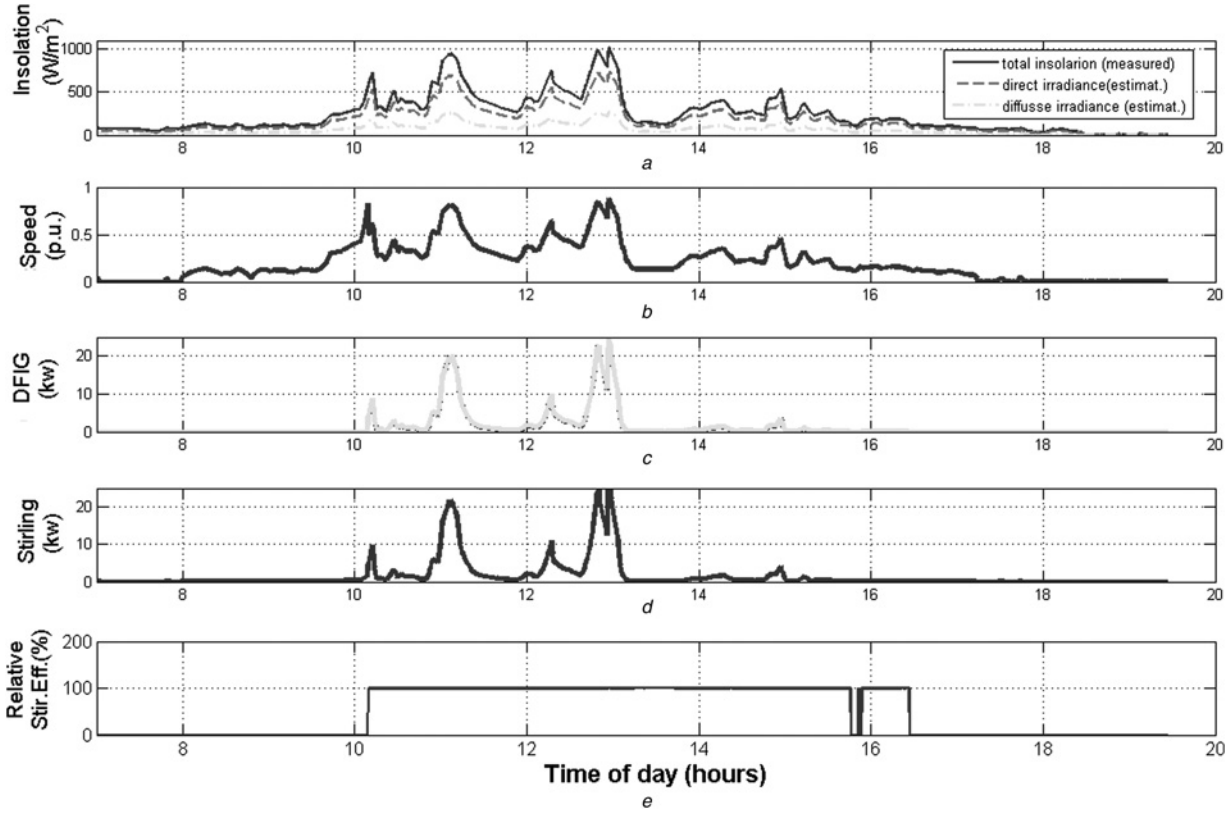

Fig. 14 *Dynamic response with MPPT (open loop) for real insolation data of one cloudy day (from top to bottom)*

a Insolation
b Speed
c DFIG output power and reference
d Stirling power
e Relative electric efficiency

IET Renew. Power Gener., 2012, Vol. 6, Iss. 4, pp. 276–288
doi: 10.1049/iet-rpg.2011.0188

per minute at some time after 13 h (Figs. 14*a*–*d*). Only at the end of the day, close to 16 h, and with very low insolation values and zero effective generated power the efficiency drops (Fig. 14*e*).

With these two examples it has been demonstrated that the relative efficiency is always higher than 99.5% when generating power, therefore it can be assumed that the yearly performance will be also around this value. In order to evaluate rigorously the annual performance improvement using a variable speed system with the proposed controllers against a fixed speed, yearly statistical data should be used to reproduce the simulations. This comparison will depend on the Stirling engine torque-speed characteristic and also in the rated values of the fixed speed system.

7 Conclusions

State of the art for DS technology has been revised, showing that the current grid connected kinematic systems use induction generators at fixed speed and do not consider the capability of controlling the power by means of varying the speed of the engine, although the power-speed characteristic shows that there is an optimal speed that obtains a maximum brake thermal efficiency point for each insolation value.

This paper presents a novel approach to control DS systems when connected to a DFIG, considering the speed as a new control variable that provides a new degree of freedom to optimise the process at any operation condition.

Furthermore, two different control systems (open-loop and P&O) are proposed to achieve MPPT based on DPC, providing satisfactory results when using real insolation data as inputs.

DPC offers extremely high dynamics and it seems a very convenient strategy for controlling DFIG for DS technology because of the small inertia of the whole system. Although future research should consider including more detailed thermodynamic models or more precise models based on empirical data it is not expected to modify the main conclusions of applying the proposed control strategy based on a variable speed system as DS system power is a function of the rotational speed.

8 References

1 Mancini, T., Heller, P., Butler, B., *et al.*: 'Dish-stirling systems: an overview of development and status', *J. Sol. Energy Eng.*, 2003, **125**, pp. 135–151

2 Trieb, F., Langniß, O., Klaiß, H.: 'Solar electricity generation-a comparative view of technologies, costs and environmental impact', *Sol. Energy*, 1997, **59**, pp. 89–99

3 Stine, W.B., Diver, R.B.: 'A compendium of solar dish/stirling technology', SAND93-7026 UC-236 Unlimited Release Printed January 1994, available at http://www.osti.gov/energycitations/servlets/purl/10130410-xiVU1V/native/10130410.pdf

4 Thombare, D., Verma, S.: 'Technological development in the Stirling cycle engines', *Renew. Sustain. Energy Rev.*, 2008, **12**, pp. 1–38

5 Kongtragool, B.: 'A review of solar-powered Stirling engines and low temperature differential Stirling engines', *Renew. Sustain. Energy Rev.*, 2003, **7**, pp. 131–154

6 'Tessera Solar and Stirling Energy Systems Unveil World's First Commercial Scale SuncatcherTM Plant, Maricopa Solar, with Utility Partner Salt River Project', Press Release, Tessera Solar, January 22, 2010, available at http://tesserasolar.com/north-america/pdf/2010_01_22.pdf

7 Kalogirou, S.A.: 'Solar thermal collectors and applications', *Prog. Energy Combust. Sci.*, 2004, **30**, (3), pp. 231–295

8 Petrescu, S., Costea, M., Harman, C., Florea, T.: 'Application of the direct method to irreversible stirling cycles with finite speed', *Int. J. Energy Res.*, 2002, **26**, pp. 589–609

9 Senft, J.R.: 'Theoretical limits on the performance of stirling engines', *Int. J. Energy Res.*, 1998, **22**, pp. 991–1000

10 Formosa, F., Despesse, G.: 'Analytical model for Stirling cycle machine design', *Energy Convers. Manage.*, 2010, **51**, pp. 1855–1863

11 Poullikkas, A., Kourtis, G., Hadjipaschalis, I.: 'Parametric analysis for the installation of solar dish technologies in Mediterranean regions', *Renew. Sustain. Energy Rev.*, 2010, **14**, pp. 2772–2783

12 Karabulut, H., Yucesu, H.S., Koca, A.: 'Manufacturing and testing of a V-type Stirling engine', *Turk. J. Eng. Environ. Sci.*, 2000, **24**, (2), pp. 71–80

13 Cinar, C., Yucesu, S., Topgul, T., Okur, M.: 'Beta-type Stirling engine operating at atmospheric pressure', *Appl. Energy*, 2005, **81**, pp. 351–357

14 Kongtragool, B., Wongwises, S.: 'Performance of a twin power piston low temperature differential Stirling engine powered by a solar simulator', *Sol. Energy*, 2007, **81**, pp. 884–895

15 Kongtragool, B., Wongwises, S.: 'A four power-piston low-temperature differential Stirling engine using simulated solar energy as a heat source', *Sol. Energy*, 2008, **82**, pp. 493–500

16 Kongtragool, B., Wongwises, S.: 'Performance of low-temperature differential Stirling engines', *Renew. Energy*, 2007, **32**, pp. 547–566

17 Cinar, C., Karabulut, H.: 'Manufacturing and testing of a gamma type Stirling engine', *Renew. Energy*, 2005, **30**, pp. 57–66. Eighth Int. Stirling Engine Conf., 1997, pp. 29–38

18 Karabulut, H., Çınar, C., Oztürk, E., Yücesu, H.S.: 'Torque and power characteristics of a helium charged Stirling engine with a lever controlled displacer driving mechanism', *Renew. Energy*, 2010, **35**, (1), pp. 138–143

19 Iwamoto, S., Hirata, K., Toda, F.: 'Performance of Stirling engines', *JSME Int. J. Series B*, 2001, **44**, (1), pp. 140–147

20 Takahashi, I., Ohmori, Y.: 'High-performance direct torque control of an induction motor', *IEEE Trans. Ind. Appl.*, 1989, **25**, pp. 257–264

21 Noguchi, T., Tomiki, H., Kondo, S., Takahshi, I.: 'Direct power control of PWM converter without power source voltage sensors', *IEEE Trans. Ind. Appl.*, 1988, **34**, pp. 473–479

22 Pena, R., Clare, J.C., Asher, G.M.: 'Doubly fed induction generator using back-to-back PWM converters and its application to variable-speed wind-energy generation', *IEE Proc. Electr. Power Appl.*, 1996, **143**, (3), pp. 231–241

23 Bird, R.E., Riordan, C.J.: 'Simple simple solar spectral model for direct and diffuse irradiance on horizontal and tilted planes at the earth's surface for cloudless atmospheres', *J. Climate Appl. Meteorol.*, 1986, **25**, (1), pp. 87–97

9 Appendix

9.1 Mechanical model

Table 6 shows the mechanical parameters of the model, where Ω_{base} and S_{base} (kW) are the base units for the speed and power, respectively; H and D are the inertia and friction coefficients in base units, respectively.

9.2 Stirling engine model

Table 7 shows the power-speed characteristics of the Stirling engine model, where T_0, the extrapolated torque at zero speed, and m_i both vary with the heating.

Table 6 Mechanical parameters

Ω_{base}, rpm	S_{base}, kW	H, p.u.	D, p.u.
1500	25	0.5	0.1

Table 7 Stirling power-speed parameter values

Q_0, p.u.	m_i, N m/rpm	i_0, N m	τ, s	Ω, rpm
0–1	$-0.125Q_0(1-e^{-t/\tau})$	$75Q_0^2(1-e^{-t/\tau})$	5	0–2200

9.3 DFIG model with DPC

Table 8 shows the DFIG characteristics, where R_s, R_r are the stator and rotor resistances, respectively, L_m is the mutual inductance and, L_{ds}, L_{dr}, are the stator and rotor leakage inductance, respectively.

Table 8 dfig equivalent circuit parameter values

R_s, p.u.	R'_r, p.u.	L_m, p.u.	$L_{\sigma s}$, p.u.	$L_{\sigma r}$, p.u.	Pp
0.014	0.015	3.0	0.2	0.23	2

9.4 MPPT controllers

Table 9 shows the MPPT regulator parameters, where PI(k_p), PI(k_I) are the proportional and integral parameters of a parallel PI regulator; and T, Δ_{speed} are the running time window and constant step for the MPPT (P&O), respectively.

Table 9 Controllers parameters values

PI(k_p)	PI(k_I)	MPPT(P&O): T, ms	MPPT(P&O): Δspeed, p.u.
1.57	0.314	20	0.005

9.5 Measured insolation data details

The insolation measured data corresponds to a location of latitude 45.5875° and longitude: 10.438889° measured with the irradiation sensor CellSol 200 the days 07/08/2011 (cloudy day) and the 22/08/2011 (sunny day). The direct beam and diffuse irradiance have been estimated for this location and dates by correlation of the measured data with the simulation tool [23].

doi: 10.1049/iet-rpg.2011.0188